Study of the surface pressure fluctuations generated by waves and turbulence in the nocturnal boundary layer during SABLES2006 field campaign

Samuel VIANA[1], Carlos YAGÜE[1], Gregorio MAQUEDA[2] and Gema MORALES[3]

[1] Dpto. de Geofísica y Meteorología. Universidad Complutense de Madrid, Spain
(savianaj@fis.ucm.es, carlos@fis.ucm.es)

[2] Dpto. de Astrofísica y Ciencias de la Atmósfera. Universidad Complutense de Madrid, Spain
(gmaqueda@fis.ucm.es)

[3] Instituto Nacional de Meteorología, Spain
(gmorales@inm.es).

(Received 25 April 2007; received in revised form 20 June 2007; accepted 22 June 2007)

ABSTRACT:
Small-scale, short-period surface pressure fluctuations are perhaps one of the less studied features in the atmospheric boundary layer (ABL). These perturbations can be produced by fast turbulent motions and also by the propagation of internal-gravity waves generated close to the ground when stability is present. In this work nocturnal data from SABLES2006 field campaign is analyzed in order to characterize the wave-like structures detected during the most stable periods of the campaign by means of a wavelet analysis. In addition, we will relate the spectral characteristics of surface pressure fluctuations to the turbulent and stability parameters measured from tower data.
Key words: static pressure fluctuations, gravity waves, turbulence, nocturnal boundary layers, microbarometers, wavelets.

Estudio de las Fluctuaciones de Presión Superficial Generadas por Ondas y Turbulencia en la Capa Límite Atmosférica Nocturna durante la Campaña SABLES2006

RESUMEN:
Las fluctuaciones de presión de período corto o pequeña escala son, quizá, de los aspectos menos estudiados en la capa límite atmosférica (ABL). Estas perturbaciones se producen por rápidos movimientos turbulentos y por la propagación de ondas internas generadas cerca del suelo en presencia de estabilidad. En este trabajo se han analizado datos nocturnos obtenidos en la campaña de campo SABLES2006, con objeto de caracterizar, por medio de un análisis de tranformada *wavelet,* los eventos detectados con estructuras ondulatorias durante los períodos de mayor estabilidad de la campaña. También se relacionarán las características espectrales de las fluctuaciones de la presión en superficie con los parámetros turbulentos y de estabilidad obtenidos de los datos de una torre meteorológica.
Palabras clave: fluctuaciones de presión estática, ondas de gravedad, turbulencia, capa límite nocturna, microbarómetros, *wavelets*.

1. INTRODUCTION

Atmospheric pressure is one of the main basic flow variables, which has been intensively measured since the invention of the barometer by Torricelli in 1643, and whose intimate relationship with synoptic and mesoscale meteorology has been thoroughly studied since the establishment of modern meteorology in the 19th century. On the other hand, small scale static pressure fluctuations produced in the atmospheric boundary layer (ABL) are much more difficult to measure and are therefore much less understood. These fluctuations can be due to turbulent motions and also to the propagation of waves of different types (gravity waves, Kelvin-Helmholtz instabilities, etc), produced by different mechanisms such as orographic forcing, fronts, convective forcing, geostrophic adjustment, shear instability, etc (Ramis and Montserrat, 1991). The typical amplitude of the pressure fluctuations related to waves is in the range of 0.01-0.1 hPa (Nappo, 2002) with a periodicity ranging from 1 to 40 minutes (Stull, 1988), although some episodes of intense mesoscale gravity waves with amplitudes up to 2-3 hPa have been reported (Bosart and Cussen, 1973). As for the pressure fluctuations related to turbulent motions, their typical amplitude is of the order of several hundredths of hPa. Absolute pressure at ground level is of the order of 1000 hPa, therefore a sensitivity of 1 in 10^5 is needed in order to detect the weakest wavy or turbulent static pressure fluctuations in the ABL. This resolution is hardly achieved by most commercial barometers. Different techniques have been developed over the last decades in order to measure static pressure perturbations. The most primitive devices consisted in analogic or electronic manometers which measure pressure differences between open air and a reference chamber. More recent instruments have been developed based on different principles to measure pressure, such as the change in conductivity of semiconductors or the change in the molecular vibration frequency of different materials.

One additional difficulty to confront when using any of these instruments is related to dynamic pressure fluctuations (i.e., the term proportional to the velocity squared on the Bernoulli equation) which can contaminate the measurements of static pressure. To prevent this, static pressure ports are commonly used. These usually consist on two circular plates separated by a short distance, to which the pressure probe from the microbarometer is connected, so that almost all the dynamic perturbation produced by the wind is filtered. However, as explained by Wyngaard *et al*. (1994), there is a close coupling between static pressure and velocity, and even the aerodynamic perturbation of the flow caused by the insertion of the pressure port can contaminate the measured static pressure.

Measurements of static pressure fluctuations have become the most commonly used procedure for detecting and studying gravity waves. Although many aspects of gravity waves still remain to be clarified, such as their interaction with turbulence in the stable boundary layer (SBL), wave transport and mixing, etc, there exists a strong theoretical framework (i.e., the linear wave theory), and the connection between pressure fluctuations and flow variables (i.e., wind velocity components) is well understood by means of the polarization equations (Nappo, 2002). The observation of gravity waves from microbarometers is usually made at surface level, where the pressure perturbations associated with most waves are maximum (Nappo,

2002). Surface arrays of at least three microbarometers located hundreds of meters away from each other have been used during specific periods in field campaigns (Cheung and Little, 1990; Grivet-Talocia *et al*., 1999, Rees *et al*., 2000; Terradellas *et al*., 2001) or in continuous monitoring stations (Grivet-Talocia *et al*., 1999), for detecting and characterizing wave events by means of lag analysis (Nappo, 2002), cross-correlation (Rees and Mobbs, 1988), beamsteering (Denholm-Price and Rees, 1999) or methods based on wavelets decompositions (Terradellas *et al*., 2001).

On the other hand, the use of microbarometers for studying turbulent static pressure perturbations has not attracted as much attention as its use for detecting waves. The level of knowledge attained on the spectral properties of the turbulent static pressure perturbations is not comparable to the thorough understanding achieved on the spectra for wind speed components in the ABL. Although some attempts to extend Kolmogorov's local theory of turbulence (Kolmogorov, 1941) to the fluctuating pressure field have been made, the direct extension of Kolmogorov's arguments leads to theoretical results (i.e., the $k^{-7/3}$ scaling law for pressure), which have not been fully supported by experimental data under different conditions in which an inertial subrange for wind velocity (i.e., the well-known $k^{-5/3}$ scaling law) is present (Albertson *et al*., 1998). These unsuccessful results are related to the fact that pressure is not a completely local flow variable; regions far from the point where it is measured can make non-negligible contributions to the pressure fluctuations (Monin and Yaglom, 1975).

In this work, we will focus on both turbulent and wave-like characteristics of static pressure fluctuations, using data from SABLES2006 field campaign. Wavelet analysis will be used in order to detect wave activity produced during the campaign, and to characterize these waves in terms of usual wave parameters (i.e., wavelength, phase velocity, period and direction of propagation). Also, spectral calculations will be used to describe the differences established between the pressure series according to the level of stability present (evaluated through turbulence and stability parameters). Firstly, we will describe the experimental setup deployed and the database of pressure records gathered during the campaign. In section 3, the different analytical techniques to be used in the subsequent sections are presented. Section 4 is divided in two subsections. In section 4.1 we will study some of the wave events detected during the campaign, with the help of the wavelet analysis described on section 3. Section 4.2 comprises the main results extracted from Fourier analysis, regarding the relationship between fast pressure fluctuations and turbulence in the SBL. The main conclusions of this study will be drawn in section 5.

2. SITE AND MEASUREMENTS

Six PAROSCIENTIFIC 6016-B microbarometers were available during SABLES2006 (Stable Atmospheric Boundary Layer Experiment in Spain 2006) field campaign (see Yagüe *et al*., 2007; this issue), which took place from 19 June to 5 July 2006 at CIBA (Research Center for the Lower Atmosphere), located in Valladolid (Spain), on a flat and homogeneous terrain over an extensive plateau (San José *et al*., 1985). These high precision digital instruments can detect very small pressure

perturbations, of the order of thousandths of hPa. The working principle is based on the dependence of the vibrational frequency of a quartz crystal with temperature and applied pressure. A pressure transducer produces two square wave signals whose period is proportional to applied pressure and internal transducer temperature. The internal electronics of these devices integrates these signals for a certain time, to measure the periods of the pressure and temperature signals. From these periods the absolute pressure measurement is computed using the calibration formulas which are specific for each PAROSCIENTIFIC unit. The resolution of these instruments depends on the precision with which the temperature and pressure periods are determined (i.e., the integration time of the pressure and temperature signals). Therefore, higher sample rates mean less precise measurements; in this study a sampling rate of 2Hz was chosen as a compromise between having a good temporal resolution and registering small enough pressure perturbations (with this sampling rate the resolution is around 0.002 hPa). These values are quite suitable for a proper registration of any kind of wave event produced. Most of the turbulent pressure fluctuations can also be registered, although some of the information from the high-end portion of the pressure spectrum can be lost (the Nyquist frequency is 1Hz).

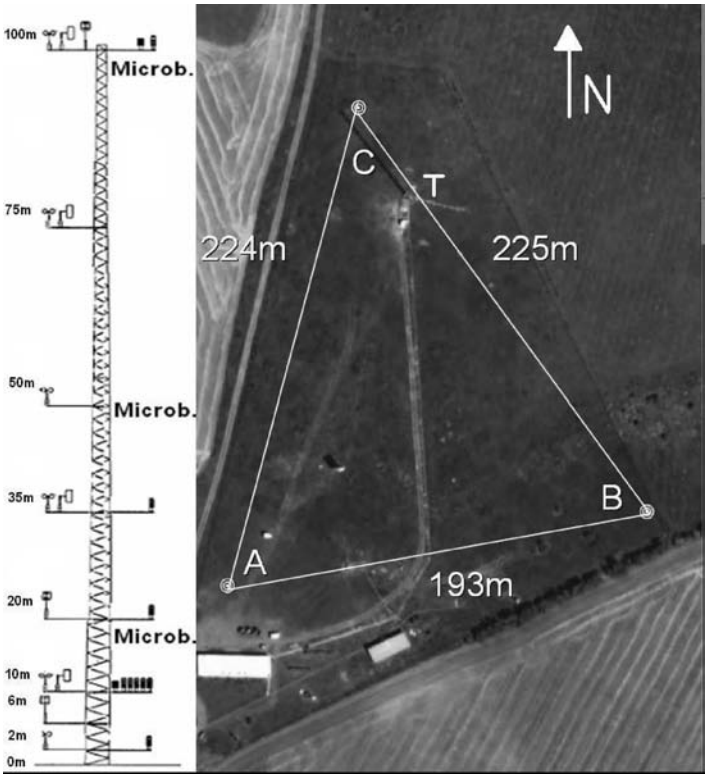

Figure 1.- Schematic view of the instrumentation deployed on the 100m tower (left), and satellite image of the CIBA site (right), with the dimensions of the surface array of microbarometers (the 100m tower "T" is located close to the northern vertex).

Three microbarometers were installed at 20, 50 and 100 m on the 100-m meteorological tower available at CIBA, and the other three (microbarometers *A*, *B* and *C*) were deployed at surface level, on a triangular array of approximately 200 m side. GILL static pressure ports were installed to avoid data contamination by dynamic pressure fluctuations. The microbarometers were installed during the first days of June, and were operative from 9 June (10 days prior the start of the campaign), until 14 July (for the microbarometers on the surface array, which was dismantled after the campaign). The microbarometers at the 100-m tower were left to complete the regular instrumentation available at CIBA. The 100-m tower is fully instrumented with cup and sonic anemometers, wind vanes, temperature and humidity sensors at different levels, etc, which make it possible to calculate turbulence and stability parameters at different levels. Only data evaluated at z=3 m is used in this study. For a more extensive description of this instrumentation, refer to Yagüe *et al*. (2007), in this issue.

With the pressure series registered at different positions at the surface, it is possible to observe the propagation of coherent structures (waves) along the CIBA site, and calculate the wave parameters (wavelength, phase speed, direction) using wavelet methods. This requires knowing the relative distances of the different surface microbarometers, which were accurately determined by a GPS system prior to the campaign. Figure 1 shows a schematic view of the instrumentation on the tower and a satellite image of the surface array, indicating the distance between the surface microbarometers.

The six microbarometers were connected to an industrial computer located close to the tower, equipped with a multiplexer card for connecting the microbarometers to six independent serial ports, using RS-485 connections. Data-logging software was installed for saving the pressure records into daily files.

In this work, surface pressure series data from the sixteen nights of the campaign are used. The nocturnal boundary layer (NBL) showed stable stratification for most of the nights during SABLES2006, with a level of stability ranging from near-neutral to strong stratification. Every night comprises data from 1800 to 0600GMT. This time selection enables our analysis to include the transition from the late daily conditions to the nocturnal ones (the sunset at CIBA is around 2000GMT at this time of the year).

3. DATA PROCESSING AND METHODOLOGY

In addition to the effects of waves and turbulence on surface pressure fluctuations, the high-resolution pressure records from the microbarometers are affected by the slow pressure trend due to the synoptic scale. On an absolute pressure plot comprising several hours of data, this trend will mask the smallest fluctuations. Even when this pressure trend is not present or is much reduced, the so-called “barometric tide” (the semi-diurnal signature of gravitational attraction of the sun and moon) can be found on daily records, also hiding the pressure fluctuations of our interest. Figure 2 shows two examples of daily evolutions of pressure under different synoptic conditions.

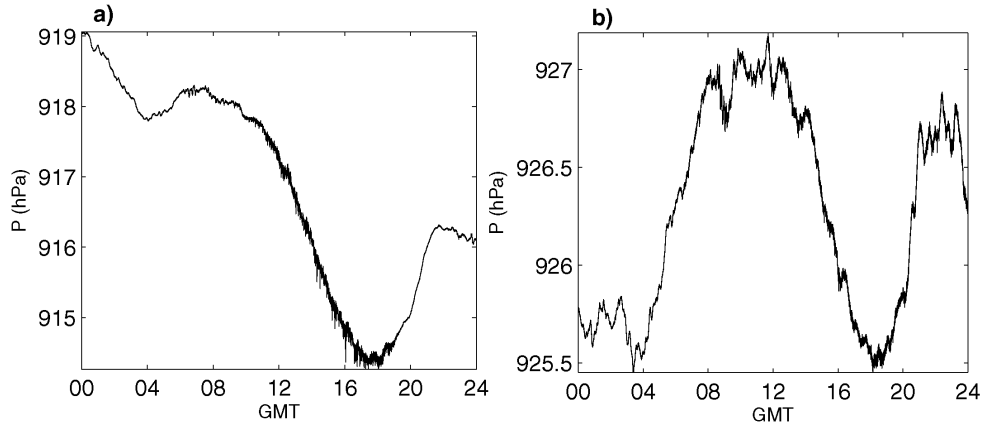

Figure 2.- Daily pressure series during (a) a synoptic trend period (23 June) and (b) a period dominated by "barometric tide" (11 July).

In order to suppress from the pressure records all the perturbations not related to the objectives of this study, some trend removal technique must be applied. Different filtering methods are available (e.g., a high pass filter can be applied, a running-mean subtracted, or the pressure fluctuations can be calculated as the difference between the microbarometer pressure and the pressure measured by a standard low-resolution barometer). We chose the high-pass filter, which has the best spectral response and effectively removes the desired spectral components on all range of amplitudes (Denholm-Price and Rees, 1998). The specific high-pass filter chosen (a first order Butterworth filter) has a flat spectral response up to the cut-off frequency, which allows us to preserve all the characteristics of the pressure fluctuations. We have chosen a cut-off frequency of $f=1/3600\ s^{-1}$, which will remove any contribution from timescales larger than one hour.

Figure 3 shows two examples of trend-removed pressure series corresponding to the absolute pressure record shown on Fig 2b. A simple visual inspection of the filtered pressure series can help to identify periods with low turbulent activity and some traces of slow wave-like fluctuations (Fig. 3a), and periods with faster perturbations due to turbulence (Fig. 3b). The high-pass filtering helps us to select the most appropriate sections of data for the wavelet analysis (especially when the wave-related activity occurs during periods with steep pressure trends); therefore the described filtering process has been routinely used before applying any of the methods detailed in the next subsections.

3.1. WAVELET TRANSFORM AND DERIVATION OF WAVE CHARACTERISTICS.

The Wavelet Transform (WT), which acts as a local Fourier decomposition, provides a simultaneous representation of the series in the time and frequency

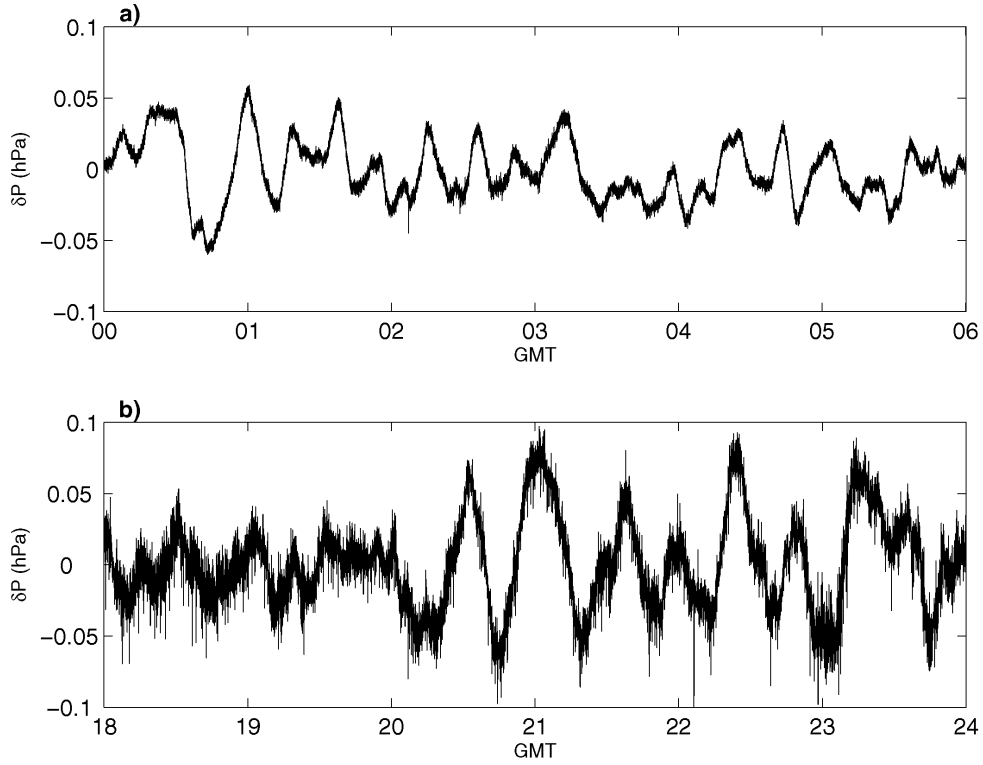

Figure 3.- Filtered pressure series corresponding to the absolute pressure series on Fig. 2b from 0000 to 0600 GMT (a) and from 1800 to 2400 GMT (b).

domains, showing which frequencies or periods are present and when they are present. The wavelet transform coefficients of a time series *f(t)* are defined as (Dabeuchies, 1991):

$$F(s, \tau) = \int_{-\infty}^{\infty} f(t)\ \Psi^{*}_{s\tau}(t)dt \tag{1}$$

where * means complex conjugation, s and τ are the scale (dilatation) and time (translation) parameters, and $\Psi_{s\tau}(t)$ is the wavelet function for a given scale and time. Functions $\Psi_{s\tau}(t)$ are generated from a mother wavelet $\Psi(t)$ according to the expression:

$$\Psi_{s,\tau}(t) = \frac{1}{\sqrt{|s|}}\ \Psi\left(\frac{t-\tau}{s}\right) \tag{2}$$

The square of the wavelet coefficients (squared modulus) is the wavelet equivalent to the Fourier power spectrum, but it is common to use the wavelet energy density per time and scale unit, which is defined as:

$$e_{s,\tau} = \frac{\left|\Psi_{s,\tau}(t)\right|^2}{s^2\, C_\Psi} \tag{3}$$

In this expression, C_ψ is a constant obtained from the admissibility condition, a constraint related to the specific mother wavelet chosen, which must fulfil some requirements (to have zero mean and to be well localized in time and Fourier space) to be appropriate for a wavelet analysis (Farge, 1992). In this study we have used the Morlet wavelet (a complex function consisting on a plane wave modulated by a Gaussian), which has a fixed relationship between scales (s) and equivalent Fourier periods (T), and has been widely used for the analysis of geophysical time series (Torrence and Compo, 1998; Cuxart *et al*., 2002). Choosing a complex mother wavelet has the advantage that the WT produces complex coefficients for every instant τ and scale s, from which the phases (φ) can be calculated. Given at least 3 time series of a variable measured at different points (i=1,2,3…) of the surface, when spectral peaks in the WT appear on certain periods T (or associated frequencies ω) and time intervals, the phases of the WT coefficients inform about the passage of the coherent structures along the surface array:

$$\varphi_i = k_x\, x_i + k_y\, y_i - \omega t \tag{4}$$

Here x_i and y_i denote the positions of the different instruments on a horizontal plane at the surface, and (k_x,k_y) are the components of the wavenumber vector. By solving the system formed by the phase differences (Terradellas *et al*., 2001):

$$\begin{aligned} \varphi_2 - \varphi_1 &= k_x\,(x_2 - x_1) + k_y\,(y_2 - y_1) \\ \varphi_3 - \varphi_1 &= k_x\,(x_3 - x_1) + k_y\,(y_3 - y_1) \end{aligned} \tag{5}$$

one can deduce the wavenumber vector components, from which the rest of the parameters (wavelength λ, phase velocity c, direction of propagation α) of the wave-like coherent structure can be derived:

$$\begin{aligned} &\lambda = 2\pi / |k| \\ &\alpha = tan^{-1}\,(k_y/k_x) \\ &c = \lambda / T \end{aligned} \tag{6}$$

Before applying this methodology for a given region of high wavelet modulus, some significance testing must be made. We followed the method by Terradellas *et al*. (2001), based on Torrence and Compo (1998), to assign statistical significance to the spectral peak for which the wave parameters will be calculated. A background mean spectrum $e_m(T)$ is calculated by averaging the WT energy density coefficients ($e_{s,\tau}$) for every scale (or period). It is assumed that the WT energy density can be expressed as the sum of the squares of two variables for a given period, both normally distributed, with zero mean and σ^2 variance. From statistical reasoning, it can be deduced that e/σ^2 will be Chi-square distributed with two degrees of freedom. Then the 95% confidence threshold for e can be constructed as:

$$e_{0.95}(T) = \frac{e_m(T)\,\chi_2^2(0.95)}{2} \tag{7}$$

The significance of every coefficient $e_{s,\tau}$ is therefore tested against this value, which makes possible to define the statistically significant areas on the WT plots, i.e., areas where the energy density exceeds the 95% confidence level. This type of significance testing, in which the significance of every point in the time-period plane is tested individually, is known as "pointwise" significance testing, as opposed to the "areawise" significance testing, which takes into account the size of the significant regions, to confront the problem of the false positive results which often appear when the "pointwise" method is applied (Maraun *et al*., 2007). We judge the "pointwise" testing to be reliable enough for our objectives, since the significance of the spectral peaks to study will be reinforced by other supporting evidences from tower data, such as high Richardson number, low levels of turbulence, etc.

3.2. HIGH-FREQUENCY INTEGRATED VARIANCE

We developed a methodology for studying the relationship between the short-period pressure fluctuations (which are expected to be produced by turbulence) and the turbulent and stability parameters calculated from tower data. Other studies (Shaw *et al*., 1989) explored this relationship calculating the root-mean-square or variance of pressure series data. Since the main correlation between the pressure and the near-surface wind field is due to the high-frequency component of the pressure series, their results were less scattered when the pressure series were pre-filtered by subtracting a 40s running average to the data. However Denholm-Price and Rees (1998) showed the weakness of the running average filter, which fails to give a neutral spectral response over frequencies far from the corresponding to the cut-off frequency, therefore we rejected this method. Instead of using the running-mean method, a Fourier transform was applied to 30-minutes sub-series of our filtered nocturnal data for the whole campaign. The smoothed spectra of every sub-series were obtained

using the spectral splicing technique described in Kaimal and Finnigan, (1994). From the coefficients of every spectra, *S(f)*, a partially integrated variance was calculated:

$$\sigma^2_{P70s} = \int_{f_0}^{f_{Nyquist}} S(f)df \tag{8}$$

This partially integrated variance describes the contribution by the higher frequencies (periods shorter than 70s) to the total variance of the 30-min subseries. The specific integration limit (f_0=1/70 s^{-1}) on eq. (8) was chosen in order to exclude possible contributions by the pressure perturbations generated by the wave-like structures with the lower periods (of the order of one minute). For convenience, we will use its square root, σ_{P70}, which we define as the high-frequency contribution to the standard deviation. In section 4.2 we will relate σ_{P70} to the mean values of turbulent and stability parameters: friction velocity (u_*), turbulent kinetic energy (*TKE*), stability parameter (*z/L*) and gradient Richardson number (Ri_g), evaluated at z=3 m from tower data (for further details on the calculation of these parameters, see Yagüe *et al*., 2007, this issue.

4. RESULTS

4.1. WAVE EVENTS DETECTED DURING SABLES2006

Figures 4-5 comprise the WT and wave parameters of a wave event encountered during SABLES2006. The background conditions for this event were: supercritical Richardson number, weak and intermittent turbulence and the presence of low-level jets (LLJ) and counter-gradient fluxes of heat and momentum (where eddy exchange coefficients of momentum, K_h, and heat, K_m, are negative). During this event, produced on June 26 from 0100-0500GMT, the filtered pressure series from the surface array show a characteristic wavy pattern without important traces of turbulent activity. Figure 4 shows the pressure series and results from wavelet analysis for microbarometer "A"; the results from the other two microbarometers look very similar. The WT (Fig. 4b) show two main peaks of energy density, centred round 0230GMT and 0345GMT, with a periodicity of around 18 and 25 minutes, respectively. The black solid line on Fig. 4b encloses the area where the WT energy density exceeds the 95% confidence level (dashed line on Fig. 4c) according to the "pointwise" significance testing described on section 3.1. The mean spectrum used as background spectrum for the significance test (solid line on Fig. 4c) was calculated from the WT coefficients from 2100GMT to 0700GMT. Only the first peak on Fig. 4b has proved statistically significant. This peak fits with the secondary peak with periodicity around 18 minutes found in the mean spectrum of WT energy density on Fig. 4c. The stronger peak in the mean

spectrum located around 30 minutes, corresponds to an earlier region of high WT energy density found around 2300GMT, which must be discarded for further analysis, since it resulted not to be significant, besides the fact that background conditions (subcritical Richardson number, a local increase in *TKE*, K_h & K_m, and a more "turbulent" pressure fluctuation signal) are not indicative of wave activity. Therefore we focus our analysis on the first spectral peak on Fig. 4b, for which the WT modulus and wave parameters obtained after solving the system on eq. (5) are shown in Figs. 5a-d. The maximum in the WT modulus is used to locate the representative period in order to evaluate the wave parameters. Notice that the wave parameters on Figs. 5b-d show a slow variation close to the time and period where the maximum in the WT modulus is located, which gives confidence to the values found. When the opposite is true (i.e., when contour lines are tightly distributed), the structures on the different points of the array might be showing an independent evolution, and the spectral peak can be a false significant one (Terradellas *et al*., 2001). From these wave parameters it can be concluded that the coherent structure detected propagated towards SE with a period around 22 minutes, a phase speed in the range of 7.5 – 9 m s^{-1} and an estimated wavelength between 9 and 12 km approximately.

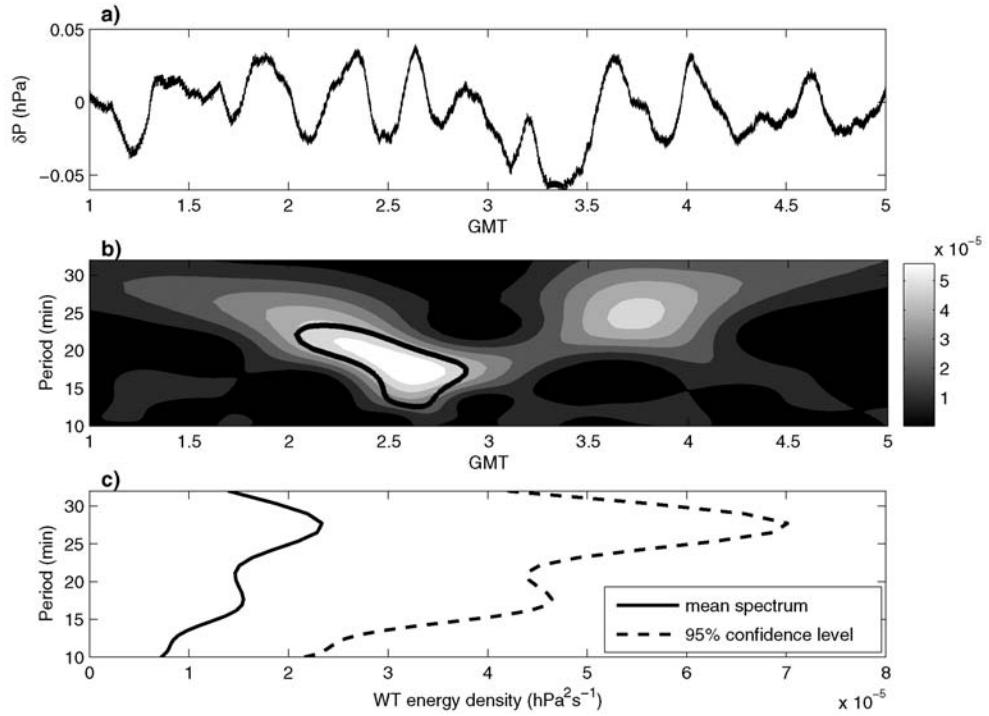

Figure 4.- Pressure fluctuations (a), WT energy density (hPa^2s^{-1}) (b) and mean spectrum and confidence level (c), for the wave event detected on 26 June.

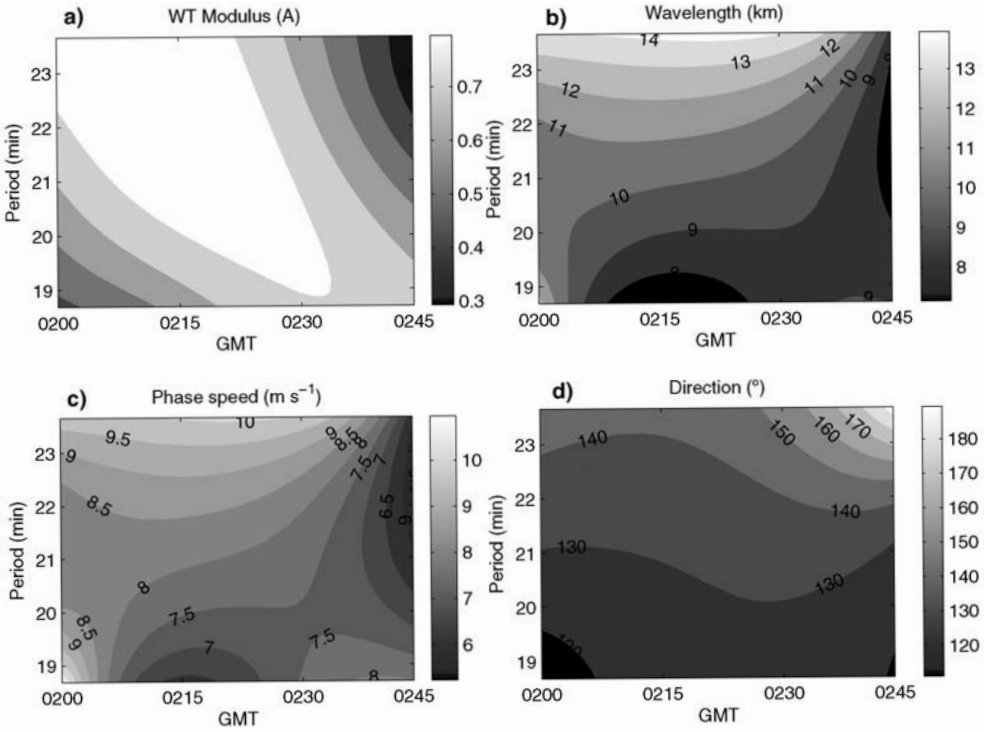

Figure 5.- WT modulus (a), wavelength (b), phase speed (c) and direction of propagation (d) for the coherent structure detected on 26 June at 0215GMT.

4.2. RELATIONSHIP BETWEEN TURBULENT PARAMETERS AND σ_{P70}

Figure 6 shows the dependence of σ_{P70} with *TKE*, u_*, *z/L* and Ri_g evaluated at z= 3m during the nocturnal periods from SABLES2006. We calculated σ_{P70} for 30-min sub-series of pressure fluctuations, overlapping every 15 minutes. The averaging length used for the calculation of turbulence and stability parameters is 5 minutes. Every value of σ_{P70} is assigned to the average value of these parameters during the central 15 minutes of every sub-series. In this way we increase the number of pairs of data in our scatter plots. The data have been grouped into different intervals of the x-axis variable (each one containing approximately the same number of individual data pairs), which is plot with a logarithmic x-axis. The points shown are the geometric means of the points inside each interval, and vertical error bars (calculated as the standard deviation) are shown. The original points are also plotted (shaded). Figures 6a&b show that σ_{P70} increases progressively with increasing *TKE* and u_*, approaching values close to the systematic error of the microbarometers (0.001hPa) when the level of turbulence is very low ($TKE < 0.1$ m^2 s^{-2}, $u_* < 0.1$ m s^{-1}). If a linear x-axis is used with the data on Fig. 6a, a well defined linear evolution between *TKE* and σ_{P70} can be traced (not shown).

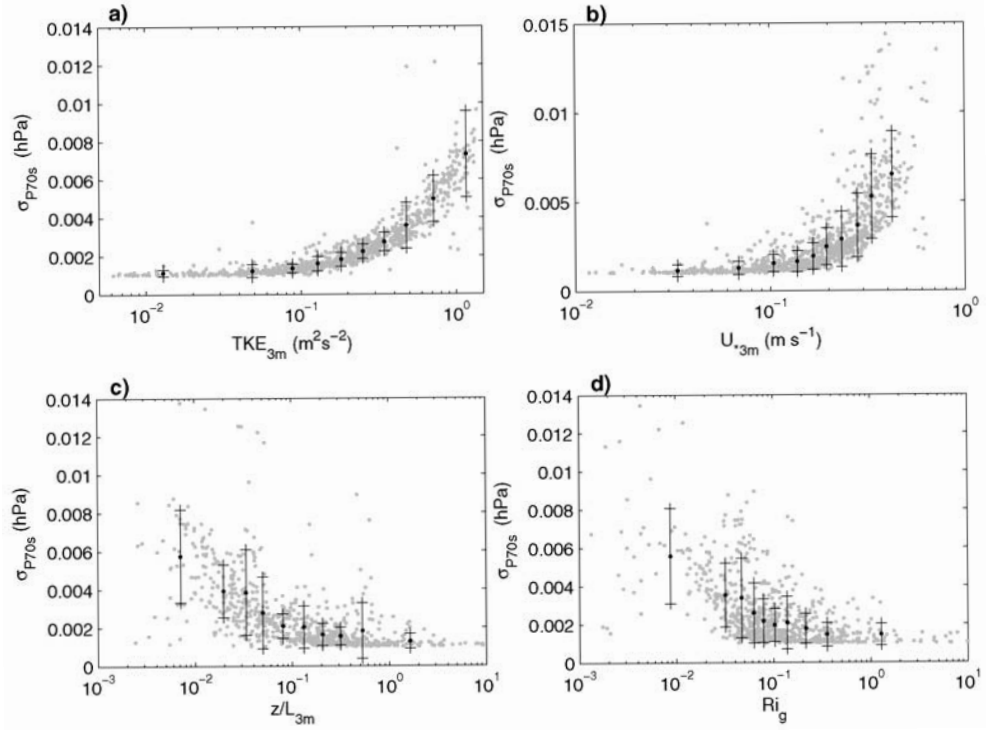

Figure 6.- Dependence of σ_{P70} with TKE (a), u_* (b), z/L (c) and Ri_g (d).

A linear relationship was also obtained by Shaw *et al*. (1990) between the mean square turbulent velocity and standard deviations of 30-minutes pressure records (high-pass filtered by subtracting a running average of 40s duration) over a deciduous forest. This linear relationship is explained in terms of the Poisson equation for pressure:

$$\frac{\partial^2 p}{\partial x_i^2} = -\rho \left[2 \frac{\partial \bar{u}_i}{\partial x_j} \frac{\partial u'_j}{\partial x_i} + \frac{\partial^2}{\partial x_i \partial x_j} (u'_i u'_j - \overline{u'_i u'_j}) + \frac{g}{T} \frac{\partial \theta'_i}{\partial x_i} \delta_{i3} \right] \qquad (9)$$

The three terms on the right hand represent the contribution to pressure fluctuations by the interaction of turbulence with the mean shear, the interaction of turbulence with itself, and the thermal disturbances due to ground heating, respectively (Katul *et al*., 1996). In the integrated form of this equation, all terms contain a velocity squared, except for the buoyancy term. However most of the times the height where the surface microbarometers are located ($z=1$ *m*) will fall inside the dynamic sublayer ($z<L$, L=Monin Obukhov length), where the influence of thermal effects is negligible and so the buoyancy term. Thus, the pressure fluctuations close to the ground are mainly produced by dynamical effects. Many

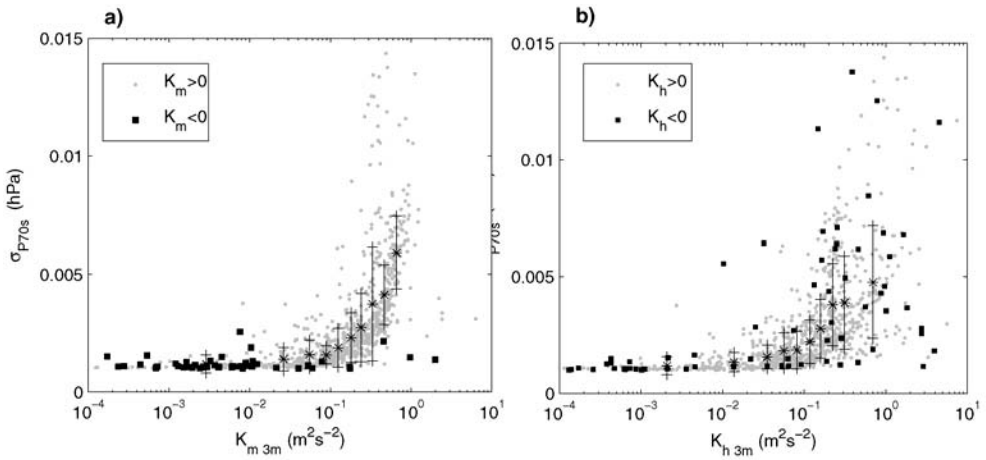

Figure 7.- Dependence of σ_{P70} with K_m*(a)* and K_h*(b)* evaluated at z=3m.

theoretical and experimental results (Kraichnan, 1956; Panton and Linebarger, 1974) identify the interaction of turbulence with the mean shear as the main source for turbulent pressure fluctuations in the dynamic sublayer.

As expected, both stability parameters on Figs. 6c&d show an inverse dependence with σ_{P70} compared to that found for turbulent parameters. Both formulas for Ri_g and *z/L* include the wind shear in the denominator (the former explicitly through $\partial\bar{u}/\partial z$, the latter indirectly through u_*), which explains the decrease of σ_{P70} with increasing Ri_g and *z/L*. The scatter in these plots is greater than for *TKE* and u_*, especially for low values of Ri_g and *z/L*. This is related to the commented prevalence of dynamical effects over thermal effects on the dynamic sublayer: Ri_g and *z/L* include both effects on stability, but only one is affecting the pressure fluctuations in the dynamic sublayer. When $z/L \ll 1$, the dynamic sublayer is thicker and the level of measurements is well inside this layer. Consequently, only the wind shear is controlling the turbulent pressure fluctuations, and the presence of the thermal effect on *z/L* can be seen as "noise" which increases the scatter. As *z/L* increases, *L* becomes of the same order of magnitude than *z*, and the thermal effects become more important as the level of measurement can be outside of the dynamical sublayer ($z>L$). The last term on eq. (9) can't be ignored, σ_{P70} is well controlled by *z/L* in this regime, therefore the scatter is reduced. This argumentation can be extended to Ri_g, since both stability parameters are linked by the similarity theory.

5. CONCLUSIONS

We have studied the two main sources of pressure fluctuations in the atmospheric boundary layer under different conditions from near-neutral stratification to moderate stability. The main conclusions of this study are:

— A wave event found during one moderately stable night from SABLES2006 has been characterized by means of wavelet analysis. An estimation of the characteristic parameters of this structure, whose period was around 22 minutes, have been calculated. Background conditions include the presence of a LLJ, supercritical Richardson number and low levels of turbulence.

— Under near-neutral to moderate stability, the high-frequency spectral characteristics of the surface pressure fluctuations in SABLES2006 are mainly controlled by the wind shear in the dynamical sublayer, and σ_{P70} increases with increasing u_* and *TKE*. A linear relationship between TKE and σ_{P70} has been found, in agreement with previous studies.

— Stability parameters as *z/L* and Ri_g fail to control σ_{P70} in the dynamic sublayer, showing important scatter when the SBL shows neutral or weakly stable conditions, due to the presence of an independent term (the thermal effect) in the definitions of these parameters. In the regime of moderate to strong stability, this term comes into play and the scatter is reduced.

6. ACKNOWLEDGEMENTS

This research has been funded by the Spanish Ministry of Education and Science (projects CGL2004-03109 and CGL2006-C03-03). IV PRICIT program (supported by CM and UCM) has also partially financed this work through the Research Group "Micrometeorology and Climate Variability" (nº 910437). Special thanks are due to Dr. Javier Peláez for his technical support along the campaign. We are also indebted to Prof. Casanova, Director of the CIBA, for his kind help. The location of the three surface microbarometers from GPS was done by Prof. Gracia Rodríguez Caderot (Universidad Complutense de Madrid).

REFERENCES

ALBERTSON, J.D., G.G. KATUL, M.B. PARLANGE & E.B. EICHENGER (1998). Spectral scaling of static pressure fluctuations in the atmospheric surface layer: the interaction between large and small scales. *Physics of Fluids*, 10, 1725-1732.

BOSART, L.F., & J.P. CUSSEN JR (1973). Gravity wave phenomena accompanying east coast cyclogenesis. *Monthly Weather Review*, 101, 446-454.

CHEUNG, T.K. & C.G. LITTLE (1990). Meteorological tower, microbarograph array, and sodar observations of solitary-like saves in the nocturnal boundary layer. *Journal of Atmospheric Sciences,* 47, 2516 - 2536.

CUXART, J., G. MORALES, E. TERRADELLAS, and C. YAGÜE, (2002). Study of Coherent Structures and Estimation of the Pressure Transport Terms for the Nocturnal Stable Boundary Layer, *Boundary-Layer Meteorol*. 105, 305–328.

DABEUCHIES, I. (1992). *Ten Lectures on Wavelets*. Society for Industrial and Applied Mathematics, Philadelphia, PA, 354 pp.

DENHOLM-PRICE, J.C.W. & J.M. REES (1998). A practical example of low-frequency trend removal. *Boundary-Layer Meteorol.,* 86, 181–187.

FARGE, M. (1992). Wavelet Transforms and their Applications to Turbulence. *Annu. Rev. Fluid Mech*. 24, 395–457.

GRIVET-TALOCIA, S., F. EINAUDI, W.L. CLARK, R.D. DENNETT, G.D. NASTROM, & T.E. VANZANDT (1999). A 4-yr climatology of pressure disturbances using a barometer network in central Illinois. *Monthly Weather Review*, 127, 1613-1629.

KATUL, G. G., J.D. ALBERTSON,C.-I. HSIEH, P.S. CONKLIN, J.T. SIGMON, M.B. PARLANGE & K.R. KNOWERR (1996). The "inactive" eddy-motion and the large-scale turbulent static pressure fluctuations in the dynamic sublayer. *J. Atmos. Sci.,* 53, 2512-2524.

KOLMOGOROV, A.N. (1941). Local structure of turbulence in an incompressible fluid at very high Reynolds numbers. *Dokl. Accad Nauk*. URSS, 30, 299-303

KRAICHNAN, R. H. (1956). Pressure field within homogeneous anisotropic turbulence. *J. Acoust. Soc. Am*., 28, 64-72

MARAUN, D., J. KURTHS & M. HOLSCHNEIDER, (2007). Nonstationary Gaussian Processes in Wavelet Domain: Synthesis, Estimation and Significance Testing. *Phys. Rev. E* 75, 016707

MONIN, A.S., & A.M. YAGLOM (1975). *Statistical Fluid Mechanics.* MIT Press, Cambridge, Vol. 2, p. 874.

NAI-PING, L., W.D. NEFF, & J.C. KAIMAL (1983). Wave and turbulence structure in a disturbed nocturnal inversion. *Boundary-Layer Meteorol.*, 26, 141-155

NAPPO, C. J. (2002). *An introduction to atmospheric gravity waves*, Academic Press, California, 276pp.

PANTON, R.L. & J.H. LINEBARGER, (1974). Wall pressure spectra calculations for equilibrium boundary layers. *J. Fluid Mech.*, 65, 261-275.

RAMIS, C. & S. MONSERRAT (1991). Ondas Gravitatorias troposféricas. Estudio de su estabilidad mediante modelos de capas. *Fisica de la Tierra*, 3, 245-282. Ed. Univ. Compl. Madrid

REES, J.M. & S.D. MOBBS (1988). Studies of internal gravity waves at halley base, antarctica, using wind observations. *Quarterly Journal of the Royal Meteorological Society*, 114, 939-966.

REES, J.M., J.C.W. DENHOLM-PRICE, J.C. KING & P.S. ANDERSON (2000). A climatological study of internal gravity waves in the atmospheric boundary layer overlying the brunt ice shelf, Antarctica. *Journal of Atmospheric Sciences*, 57, 511-526.

SAN JOSÉ, R., J.L CASANOVA, R. E. VILORIA & J. CASANOVA (1985). Evaluation of the turbulent parameters of the unstable surface boundary layer outside Businger's range. *Atmos. Environ.*, 19, 1555-1561.

SHAW, R.H., K.T. PAW, X.J. ZHANG, W. GAO, G. HARTOG & H. H. NEUMANN (1990). Retrieval of turbulent pressure fluctuations at the ground surface beneath a forest. *Boundary Layer Meteorology*, 50, 319-338

TORRENCE, C. and G.P. COMPO, (1998). A Practical Guide to Wavelet Analysis. *Bull. Amer. Meteor. Soc.*, 79, 61-78.

WYNGAARD J.C., A. SIEGEL & J.M. WILCZAK (1994). On the response of a turbulent-pressure probe and the measurement of pressure transport. *Boundary-Layer Meteorol.*, 69, 379-396.

STULL, R.B (1988). *An introduction to boundary layer meteorology*. Kluwer Academic Publishers, Dordrecht, 666pp.

TERRADELLAS, E., G. MORALES, J. CUXART & C. YAGÜE (2001). Wavelet methods: application to the study of the stable atmospheric boundary layer under non-stationary conditions. *Dyn. Atmos. Oceans.,*34**,** 225–244

YAGÜE, C., G. MAQUEDA & J.M. REES (2001). Characteristics of turbulence in the lower atmosphere at Halley IV Station, Antarctica. *Dyn. Atmos. Oceans*, 34, 205–223

YAGÜE, C., S. VIANA, G. MAQUEDA & J.M. REDONDO (2006). Influence of stability on the flux-profile relationships for wind speed, φ_m, and temperature, φ_h, for the stable atmospheric boundary layer. *Nonlinear Processes in Geophysics*, 13, 185–203

YAGÜE, C., S. VIANA, G. MAQUEDA, M.F. LAZCANO, G. MORALES & J.M. REES (2007). A study on the nocturnal atmospheric boundary layer: SABLES2006. *Física de la Tierra*, 19, this issue.